

A CO Survey of Young Planetary Nebulae¹

P. J. Huggins², R. Bachiller³, P. Planesas³, T. Forveille^{4,5}, P. Cox⁶

ABSTRACT

We report the results of a sensitive survey of young planetary nebulae in the CO $J = 2 - 1$ line that significantly increases the available data on warm, dense, molecular gas in the early phases of planetary nebula formation. The observations were made using the IRAM 30 m telescope with the 3×3 pixel Heterodyne Receiver Array (HERA). The array provides an effective means of discriminating the CO emission of planetary nebulae in the galactic plane from contaminating emission of interstellar clouds along the line of sight. 110 planetary nebulae were observed in the survey and 40 were detected. The results increase the number of young planetary nebulae with known CO emission by approximately a factor of two. The CO spectra yield radial velocities for the detected nebulae, about half of which have uncertain or no velocity measurements at optical wavelengths. The CO profiles range from parabolic to double-peaked, tracing the evolution of structure in the molecular gas. The line widths are significantly larger than on the Asymptotic Giant Branch, and many of the lines show extended wings, which probably result from the effects on the envelopes of high velocity jets.

Subject headings: circumstellar matter — planetary nebulae: general — stars: AGB and post-AGB — stars: mass loss — stars: radio lines

1. Introduction

Observations of molecular gas have played a key role in developing our current understanding of stellar evolution from the Asymptotic Giant Branch (AGB) through the planetary

¹Based on observations carried out with the IRAM 30 m telescope. IRAM is supported by INSU/CNRS (France), MPG (Germany), and IGN (Spain).

²Physics Department, New York University, 4 Washington Place, New York NY 10003

³IGN Observatorio Astronómico Nacional, Apartado 112, E-28003 Alcalá de Henares, Spain

⁴Observatoire de Grenoble, B.P. 53X, 38041 Grenoble Cedex, France

⁵Canada-France-Hawaii Telescope, PO Box 1597, Kamuela, HI 96743

⁶Institut d'Astrophysique Spatiale, Université de Paris Sud, 91405 Orsay, France

nebula (PN) phase. Stars evolving on the upper AGB undergo an increasing rate of mass loss which forms a dense, slowly expanding circumstellar envelope of dust and molecular gas. The mass loss eventually terminates the evolution on the AGB, and when the surface temperature of the star becomes high enough to emit a significant flux of ultraviolet radiation ($T \gtrsim 30,000$ K), it begins to photo-ionize the circumstellar material and form an optically visible PN.

Observations of neutral gas around bona fide PNe have been crucial in the development of this general scenario, and numerous atomic and molecular species have been observed. These include H I, C I, O I, and other neutral atoms (e.g., Rodriguez, Goss, & Williams 2002; Bachiller et al. 1994; Liu et al. 2001; Dinerstein, Sneden, & Uglum 1995), as well as H₂ (e.g., Kastner et al. 1996), OH (e.g., Zijlstra et al. 2001), CO (e.g., Huggins et al. 1996), and other, rarer molecular species such as HCO⁺ and CN (e.g., Bachiller et al. 1997). Millimeter CO emission has proved to be the most generally useful probe of the warm molecular component of the neutral gas for the same reasons that it is a standard probe of the precursor AGB envelopes: CO is relatively abundant and the millimeter transitions are easily excited. It can therefore be used to study the mass, structure, and kinematics of the bulk of the molecular gas.

Most of the known CO envelopes around PNe were discovered in dedicated CO surveys carried out by Huggins & Healy (1989) using the NRAO 12 m telescope, and by Huggins et al. (1996) using the SEST 15 m and IRAM 30 m telescopes. The compilation in Table 3 of Huggins et al. (1996) lists 44 PNe detected in CO. Several of these have provided examples for detailed study at high angular resolution, and interpretation of the ensemble of the CO observations forms an integral part of the evidence for the evolutionary scenario outlined above.

Several recent lines of investigation, including optical imaging of PNe (e.g., Sahai & Trauger 1998; Lopez 2003), kinematic studies of proto-PNe (e.g., Bujarrabal et al. 2001), and observations of individual molecular envelopes (e.g., He 3-1475, Huggins et al. 2004; AFGL 618, Cox et al. 2003), have focused attention on the complex geometry of PN formation. The underlying mechanisms are not well understood, but they likely involve effects that influence the survival of, or affect the characteristics of, the molecular gas found in young PNe. Accordingly we have undertaken a deeper search for CO, especially in young PNe, to significantly extend the sample where the characteristics of the molecular gas are known.

Based on considerations of line opacity, atmospheric transparency, telescope beam size, and receiver sensitivity, the 230 GHz CO $J = 2 - 1$ line is the optimal transition for CO searches of PN envelopes, where the emission is distributed on small angular scales and is optically thin, or partially thin, in most cases. In the time since our previous survey work,

an important increase in capability at 230 GHz has been the development of multiple beam receivers. PNe are distributed close to the galactic plane, and a sensitive search in CO is inevitably contaminated by interstellar CO emission. The use of a multiple beam array on the IRAM 30 m telescope for the present survey observations proves to be a very efficient way to address this issue.

The plan of the rest of this paper is as follows. Section 2 describes the sample selection and the observations; Sections 3 and 4 present the results of the survey, in the form of a table, spectra, and comments on individual objects; and Section 5 gives a brief discussion. A detailed analysis of the results will be given in a separate paper.

2. The Survey

2.1. Survey Sample

The survey PNe were taken from the Strasbourg-ESO Catalog of Galactic PNe (Acker et al. 1992) and were chosen to include a major component of relatively young PNe with a broad range of spectroscopic characteristics. The PNe were selected to have small angular diameters (\lesssim the telescope beam size whose FWHM is $12''$), relatively high fluxes in $H\alpha$ (with a few exceptions $> 10^{-13}$ erg cm $^{-2}$ s $^{-1}$, uncorrected for reddening), and consequently moderate to high surface brightness in the Balmer lines and the radio continuum. The PNe lie close to the galactic plane, and the practical declination limit set by the telescope location is $\sim -25^\circ$. In addition, the PNe were distributed among different spectroscopic groups, based on line ratios given in the PN catalog, or updated from the literature: 1) $[O\text{ III}] \lambda 5007/H\beta < 6.0$; 2) $[O\text{ III}] \lambda 5007/H\beta > 6.0$ and $[N\text{ II}] \lambda 6584/H\alpha > 1.0$; 3) $[O\text{ III}] \lambda 5007/H\beta > 6.0$ and $[N\text{ II}] \lambda 6584/H\alpha < 1.0$. These line ratios are not very sensitive to the reddening, but are subject to uncertainties related to the slit position and size relative to the nebula. A fourth group of miscellaneous PNe (see below) was also observed as time permitted in the program.

The angular sizes of relatively young PNe are expected to be quite small at distances outside our local neighborhood ~ 1 kpc, which has been explored in CO by earlier observations. For example, the well known PN NGC 6720 (the Ring Nebula) which is used as an intermediate benchmark below, has an angular diameter of $76''$ at a distance of 450 pc (O'Dell et al. 2002), and would have an angular diameter of $\lesssim 11''$ at distances $\gtrsim 3$ kpc. More compact PNe would have even smaller angular diameters, and such objects are well suited to line searches made with single observations centered on the nebula. The average surface brightness of the PNe in the Balmer lines or the radio continuum is independent

of distance, and is a useful guide to the degree of evolution of the nebulae. For discussion here we use the surface brightness T_B at a frequency of 1.4 GHz, using the fluxes measured directly at 1.4 GHz from Condon & Kaplan (1998) or the equivalent from the (de-reddened) Balmer lines, assuming optically thin emission. The emission at 1.4 GHz becomes optically thick before that at higher radio frequencies, but high opacity affects relatively few of the PNe and this does not substantially affect our overall discussion. The distribution of T_B for the whole PN sample ranges from 4 K to $\gtrsim 10,000$ K, with 1st, 2nd and 3rd quartiles at 110 K, 800 K, and 4,200 K, respectively.

It is well known that the surface brightness of PNe roughly correlates with nebula size (e.g., Phillips 2002, and references therein), and is therefore related to the dynamical age of the nebulae. We do not discuss this in great detail but note as benchmarks that $T_B = 3,500$ K for the compact PN BD+30°3639 and $T_B = 65$ K for the more evolved PN NGC 6720, and their expansion ages based on robust proper motions measured with HST are 800 yr and 1,500 yr, respectively (Li et al. 2002; O’Dell et al. 2002). 32% of the survey PNe have $T_B \gtrsim 3,500$ K and 84% have $T_B \gtrsim 65$ K. Thus the bulk of the observed PNe, with the exception of those with the lowest values of T_B , are expected to be younger (and in many cases much younger) than ~ 2000 yr. Our selection criteria strongly discriminate against large, evolved, low surface brightness PNe. Some of these are known to retain significant CO envelopes, as exemplified by the Helix Nebula (Young et al. 1999), $T_B \sim 1$ K, age $\sim 10^4$ yr, but the objective of the present work is to study the earlier evolution of the envelopes.

It is known from our previous observations (Huggins et al. 1996) that CO envelopes of PNe show large differences which are likely related to the mass of the central stars, and possibly additional factors as well. The distribution of the survey PNe over different spectroscopic groups is intended to provide information to investigate this further. Of course the relation between age and nebula excitation is a complex one: young PNe can have a range of stellar temperatures because the speed of the temperature increase of the star depends strongly on the stellar mass (e.g., Gesicki & Zijlstra 2000). The nebula excitation is therefore not a direct measure of the nebula age, but alone, or in combination with the brightness temperature may cast light on, or serve as a predictor of the CO emission.

Based on the [O III] $\lambda 5007$ /H β line ratio the first group (40 objects) selects low excitation PNe (excitation classes $\lesssim 2$ on the scale of Webster 1975) with central star temperatures $\lesssim 45,000$ K (e.g. Kaler & Jacoby 1991). The second group (31 objects) selects higher excitation PNe with strongly enhanced [N II] emission and is likely to include the higher mass progenitor stars which pass rapidly through the low excitation phase; the third group (28 objects) acts as a control. A small, additional fourth group (11 objects) of miscellaneous PNe with incomplete spectroscopy, or with larger angular diameters and typically in the

lowest quartile of T_B , was also observed as time in the program allowed.

2.2. Observations

The survey observations were made in the CO $J = 2 - 1$ line at 230.538 GHz using the IRAM 30 m telescope at Pico Veleta, Spain, in March 2002 and May 2003.

The receiver system used was the multibeam Heterodyne Receiver Array (HERA), which consists of nine receivers arranged in a regular 3×3 grid with a spacing on the sky of $24''$. The beam size of each “pixel” at 230 GHz is $12''$ (FWHM). For a gaussian source of size $12''$ (FWHM) centered in the array, a negligible fraction ($< 1\%$) of the signal in the central pixel is recorded in the outer pixels. The backend used was the VESPA autocorrelator, which was configured to provide $225 \times 1.63 \text{ km s}^{-1}$ channels for each of the nine receivers during the 2002 observing run, and $409 \times 1.63 \text{ km s}^{-1}$ channels during the 2003 observing run. A wide spectral coverage is essential because the CO lines of PN envelopes often have broad wings and the systemic radial velocities of many of the PNe have not previously been measured at optical wavelengths (see Section 5).

The telescope pointing was regularly monitored during the observations using reference sources, and is generally expected to be accurate within $\sim 2''$, although it is somewhat more uncertain during periods of high wind or rapidly changing weather conditions. The observations were made by switching in azimuth by $4'$ using the wobbler. The spectra were calibrated using the chopper wheel technique, and the intensities are reported here as main beam temperatures, using a beam efficiency of 0.51. The velocity scale used for the spectra is heliocentric.

The coordinates of the PNe were obtained from a compilation of optical positions (Acker et al. 1992) and accurate radio positions measured with the VLA (Zijlstra, Pottasch, & Bignell 1989; Aaquist & Kwok 1990; Condon & Kaplan 1998). In almost all cases the coordinates are known to within $\sim 1''$, and in the least favorable cases to within a few arc seconds. The coordinates are therefore not a significant source of uncertainty for the observations. Nearly all the PNe lie at low galactic latitude (b), with a mean value of $|b|$ of 3.8° .

Each PN was observed centered in the array. In all cases where the envelope was detected there was no significant envelope emission in the surrounding pixels. Interstellar (IS) lines were seen along most lines of sight, and they appear as emission (if they occur in the on position) or as dips (if they occur in the off position). In some cases the lines are narrow, isolated features and there is little confusion with the PN emission. In other cases, where

there are multiple components which may be merged, comparison of all the spectra from the array is very efficient in discriminating the IS from the PN components. The spectra presented in the next section have been obtained by subtracting the average of the outer pixels from the central pixel. This has little effect on the S/N, and is helpful in reducing the strength of the IS components, especially in cases where they are fairly uniform or have a smooth gradient across the field of the array.

3. Results

110 PNe were observed in the survey and 40 were detected. The results of the observations are summarized in Table 1. Column (1) gives the PN name in galactic notation (ordered by galactic longitude); column (2) the common name; column (3) the rms noise level of the observations; columns (4)–(7) the parameters of the CO emission in the cases where the PN is detected (see below); column (8) the heliocentric velocity interval over which there is significant interstellar contamination; and column (9) comments.

The spectra of the PNe in which CO emission is detected or tentatively detected are presented in Fig. 1. It can be seen that the spectra exhibit a large range in S/N ratio and a variety of line profiles. The parameters of the emission given in Table 1 refer to the integrated line intensity (I), the heliocentric systemic velocity in CO (V_o), the line width at zero intensity (ΔV), and the peak line temperature (T_p). In the spectra where the S/N ratio is sufficiently high that the profile shape can be discerned, I is obtained by direct integration of the profile, V_o is estimated where possible from the symmetry of the line (e.g., the average velocity of the peaks of a double-peaked profile), and ΔV and T_p are determined by inspection; because the intrinsic profiles are unknown, larger values of ΔV from broad wings at or below the noise level of the spectra cannot be ruled out. In the spectra with low S/N where the profile shape cannot be discerned, the parameters are obtained by a Gaussian fit to the line; the line width given in Table 1 is the FWHM, and it is given as a lower limit to ΔV .

4. Comments on Individual Spectra

Here we comment on the individual spectra in Fig. 1, point out IS features that appear in the profiles, and compare with available optical radial velocities (V_{opt}). These are taken from the compilation by Durand, Acker, & Zijlstra (1998), except where explicitly cited. Previous CO observations at other telescopes are also noted.

002.6+04.2 (Th 3-27) Tentative $6\text{-}\sigma$ detection. V_o consistent with V_{opt} ($-135.3 \pm 10.1 \text{ km s}^{-1}$). The narrow CO spike at $V = -13 \text{ km s}^{-1}$ is IS.

003.8+05.3 (H 2-15) Tentative $5\text{-}\sigma$ detection. V_o consistent with V_{opt} ($-63.2 \pm 3.7 \text{ km s}^{-1}$).

008.3–01.1 (M 1-40) Roughly flat-topped profile with severe IS contamination; the emission at $V \gtrsim 0 \text{ km s}^{-1}$ is probably all IS. V_o consistent with V_{opt} ($-34.4 \pm 2.0 \text{ km s}^{-1}$).

008.6–07.0 (He 2-406) Double-peaked profile. V_o consistent with V_{opt} ($+28.2 \pm 5.2 \text{ km s}^{-1}$).

010.1+00.7 (NGC 6537) Strong, triangular profile, with IS contamination on the red wing. V_o of peak differs from V_{opt} ($-16.9 \pm 1.9 \text{ km s}^{-1}$) by 13 km s^{-1} , suggesting some structural asymmetry. In deep images the nebula is much more extended than the $10''$ listed in the Strasbourg-ESO catalog, but CO is seen only in the central pixel, and likely arises in the dense inner torus whose diameter in HST images is $\sim 5''$ (Huggins & Manley 2005). A broad CO(1–0) feature at -8 km s^{-1} ($+5 \text{ km s}^{-1}$ LSR) reported by Zhang et al. (2000) is significantly different from the spectrum reported here and is likely at least partly interstellar.

011.9+04.2 (M 1-32) Tentative $3\text{-}\sigma$ detection. V_o consistent with V_{opt} ($-90.6 \pm 7.6 \text{ km s}^{-1}$).

016.0–04.3 (M 1-54) V_o of the CO peak is offset by $\sim 15 \text{ km s}^{-1}$ from V_{opt} ($-47.4 \pm 4.2 \text{ km s}^{-1}$), so the tentative, second CO feature at $V = -87 \text{ km s}^{-1}$ may be part of a broad, double-peaked profile.

019.9+00.9 (M 3-53) Probably a flat-topped profile, but strong IS (spike/dip) contamination of the blue wing. V_o consistent with uncertain V_{opt} ($+20.6 \pm 14.0 \text{ km s}^{-1}$).

021.1–05.9 (M 1-63) Double-peaked profile. V_o consistent with V_{opt} ($+8.5 \pm 10.3 \text{ km s}^{-1}$).

021.7–00.6 (M 3-55) Strong, parabolic profile, with severe IS (spike/dip) contamination; emission at $V \gtrsim 40 \text{ km s}^{-1}$ is probably all IS. The broad wing to the blue appears to belong to the PN. V_o consistent with uncertain V_{opt} ($+9.7 \pm 15.0 \text{ km s}^{-1}$).

021.8–00.4 (M 3-28) Strong, double peaked profile with IS (spike) contamination on red wing and at higher velocities. A CO spectrum obtained with the SEST 15 m telescope was previously reported by Gomez, Rodriguez, & Garay (1992). V_o consistent with uncertain V_{opt} ($+4.7 \pm 15.0 \text{ km s}^{-1}$).

023.9–02.3 (M 1-59) Single component with prominent broad wings. A CO spectrum obtained with the JCMT 15 m telescope was previously reported by Gussie & Taylor (1995). Emission spike at $V = -8 \text{ km s}^{-1}$ is IS. V_o consistent with uncertain V_{opt} ($+85.9 \pm 14.0 \text{ km s}^{-1}$).

025.9–00.9 (Pe 1-14) Single component profile with series of narrow IS spike/dip features. V_{opt} is unknown.

025.9–10.9 (Na 2) Double-peaked profile. V_o consistent with uncertain V_{opt} ($+97.8 \pm 12.0 \text{ km s}^{-1}$).

031.7+01.7 (PC 20) Single-peaked profile. V_{opt} is unknown.

032.7+05.6 (K 3-4) Single peaked profile with broad wing on red side; IS spike/dip contamination on the blue wing from 0 to -18 km s^{-1} . V_{opt} is unknown.

039.8+02.1 (K 3-17) Strong, remarkably broad, roughly flat-topped profile, possibly with additional weak wings; the dips in the profile at $V = 13\text{--}18 \text{ km s}^{-1}$ are IS. V_{opt} is unknown.

043.0–03.0 (M4-14) Strong, asymmetric double-peaked profile, with broad wings. V_o consistent with uncertain V_{opt} ($+31.7 \pm 15.0 \text{ km s}^{-1}$).

047.1+04.1 (K 3-21) Tentative $5\text{-}\sigma$ detection. V_{opt} is unknown.

055.3+02.7 (He 1-1) Tentative $5\text{-}\sigma$ detection. V_o differs by $\sim 42 \text{ km s}^{-1}$ from $V_{\text{opt}} \sim -35 \text{ km s}^{-1}$ from Guerrero et al. (1999), but roughly coincides with one of the main optical components.

055.6+02.1 (He 1-2) Flat-topped or concave profile with IS spike on the blue wing at $V = -8 \text{ km s}^{-1}$. V_{opt} is unknown.

056.0+02.0 (K 3-35) Flat-topped profile with IS spike on the blue wing at $V = -8 \text{ km s}^{-1}$. A CO spectrum obtained with the NRAO 12 m telescope was previously reported by Dayal & Bieging (1996). V_o agrees with H_2O maser velocities in the core region (Miranda et al. 2001). V_{opt} ($-9 \pm 2 \text{ km s}^{-1}$, converted from LSR from Miranda et al. 2000) is offset by $\sim 12 \text{ km s}^{-1}$.

060.1–07.7 (NGC 6886) V_o consistent with very uncertain V_{opt} ($-35.8 \pm 21.1 \text{ km s}^{-1}$).

060.5–00.3 (K 3-45) Strong, double-peaked profile; narrow dip at $V = +15 \text{ km s}^{-1}$ and spike at $V = -32 \text{ km s}^{-1}$ are IS. V_{opt} is unknown.

062.4–00.2 (M 2-48) Strong, (probably) double-peaked profile, with IS contamination of red side; narrow dip at $V = -11 \text{ km s}^{-1}$ is also IS. V_o consistent with $V_{\text{opt}} \sim -15 \text{ km s}^{-1}$ in core from Lopez-Martin et al. (2002).

067.9–00.2 (K 3-52) Double or single component with broad wings affected by strong IS contamination: dips in profile at $V = -17, -4$ and $+4 \text{ km s}^{-1}$ are IS. V_{opt} is unknown.

068.3–02.7 (He 2-459) Roughly parabolic profile with IS dips just outside the red wing. The very uncertain V_{opt} ($-72.0 \pm 20.0 \text{ km s}^{-1}$) differs from V_o by $\sim 33 \text{ km s}^{-1}$. CO(1–0) features at -9 and -15 km s^{-1} ($+9$ and $+3 \text{ km s}^{-1}$ LSR) reported by Zhang et al. (2000) are likely interstellar.

069.6–03.9 (K 3-58) Strong, double-peaked profile. V_{opt} is unknown.

074.5+02.1 (NGC 6881) Probably double peaked profile, but strong IS contamination (spikes) on blue side. V_o consistent with V_{opt} ($-14.4 \pm 2.3 \text{ km s}^{-1}$).

079.6+05.8 (M 4-17) Flat-topped or concave profile. V_o consistent with very uncertain V_{opt} ($-26.0 \pm 40.0 \text{ km s}^{-1}$).

091.6–04.8 (K 3-84) Flat-topped profile. V_{opt} is unknown.

094.5–00.8 (K 3-83) Asymmetric or double-peaked profile, affected by IS contamination on red side; dip at $V = -57 \text{ km s}^{-1}$ and just beyond the red wing are IS. V_{opt} is unknown.

104.4–01.6 (M 2-53) Steep-sided, double-peaked profile. Deep IS dip at $V = -43 \text{ km s}^{-1}$ affects the extreme red wing of the profile. V_o consistent with very uncertain V_{opt} ($-62.0 \pm 40.0 \text{ km s}^{-1}$).

107.6–13.3 (Vy 2-3) Tentative 5σ detection. Line is narrow for a PN but it could be the peak of a broader unseen component. It could be IS, but it is not seen in any of the surrounding 8 pixels, and V_o consistent with well determined V_{opt} ($-49.5 \pm 3.8 \text{ km s}^{-1}$).

119.6–06.7 (Hu 1-1) Single-peaked, asymmetric profile. The well determined V_{opt} (-53.7 ± 3.0) is offset by $\sim 14 \text{ km s}^{-1}$ from the V_o peak, in the direction of the extended wing.

130.4+03.1 (K 3-92) Double-peaked profile. V_o consistent with V_{opt} ($-61.7 \pm 2.8 \text{ km s}^{-1}$).

149.0+04.4 (K 4-47) Strong, roughly parabolic profile. V_{opt} consistent with $V_{\text{opt}} \sim -37 \text{ km s}^{-1}$ from Corradi et al. (2000).

153.7–01.4 (K 3-65) Double-peaked profile; spike at $V = -26 \text{ km s}^{-1}$ is IS. V_{opt} is unknown.

184.6+00.6 (K 3-70) Flat-topped profile. V_o consistent with V_{opt} ($+26.9 \pm 4.5 \text{ km s}^{-1}$).

359.8+06.9 (M 3-37) Strong, double-peaked profile; spike at $V = -5 \text{ km s}^{-1}$ is IS. V_o consistent with V_{opt} ($-74.2 \pm 10.2 \text{ km s}^{-1}$).

5. Discussion

5.1. Detection Rates

The observations reported here significantly increase the available data on the CO envelopes of PNe. The compilation by Huggins et al. (1996) lists 44 PNe detected in CO, and only a handful of other PNe have been detected in searches in the intervening period (e.g., Josselin & Bachiller 2000). One focus of the earlier work was large, highly evolved PNe with low surface brightness. The new sample has a higher proportion (85%) of PNe with moderate to high surface brightness ($T_B \gtrsim 65$ K using the benchmark of Section 2.1), compared to 64% of the earlier compilation, and roughly doubles the number of relatively young PNe with known CO envelopes. The 70 sensitive upper limits reported here also improve and extend the earlier data on PNe where the molecular component has been destroyed.

The overall detection rate of the new sample is 36%, and the rate shows no significant variation with T_B . On the other hand, the detection rates for the spectroscopic groups 1–4 are highly non-uniform at 15%, 71%, 36%, and 18%, respectively; this variation is significantly different from that expected on the hypothesis of a uniform distribution at the 0.1% level. These results are consistent with the view that large intrinsic variations of the CO properties of the PNe (Huggins et al. 1996) dominate over evolutionary effects for the ensemble as a whole. They also indicate that the presence of a CO envelope is correlated with higher [N II] emission in the nebula. This is likely to be mainly a direct effect in which [N II] is enhanced in dense interface gas, or shocked gas often associated with bipolar flows and dense tori. It may also be partly indirect, in that higher mass progenitors, which often have an enhanced N abundance, preferentially have more massive molecular envelopes. These will be discussed in more detail in a separate paper.

5.2. Radial Velocities

The CO spectra of the 40 detected PNe provide a useful and homogeneous set of PN radial velocities (V_o in Table 1). In the cases where the CO spectrum is relatively clear of IS line contamination and the S/N is good, the uncertainty in the measured velocities is small ~ 1 – 2 km s $^{-1}$, and is limited by the intrinsic asymmetry in the line profiles. Even in cases with severe IS contamination or low S/N, the uncertainty is almost always $\lesssim 10$ km s $^{-1}$.

High or medium quality (uncertainties $\lesssim 10$ km s $^{-1}$) optical measurements of the radial velocities of the detected PNe are available in only 18 cases (see Section 4). For this set, the mean value of $V_o - V_{opt} = 5$ km s $^{-1}$ with an rms scatter of 12 km s $^{-1}$. Thus the CO

and optical measurements provide similar, robust estimates of the systemic velocity, with part of the residual scatter being real, reflecting differences in the structure of the ionized and molecular gas in the PNe. In the other 22 cases where CO is detected but the optical uncertainties are large, $\gtrsim 10 \text{ km s}^{-1}$ (10 PNe), or are non-existent (12 PNe), the CO data provide the preferred or the only available radial velocity measurements of the PNe.

5.3. Line Profiles and Widths

A striking feature of the CO spectra shown in Fig. 1 is the variety of the line profiles. They can be broadly classified into 4 basic types: (I) parabolic, similar to the CO spectra typically seen in the precursor AGB envelopes; (II) flat-topped; (III) double-peaked; and (IV) triangular, usually asymmetrical. There are also intermediate types: e.g., with a distinct but not deep concavity, between types II and III; and with strongly asymmetrical double-peaks, between types III and IV.

These different profiles probably arise from a combination of effects. The first is the evolution of the structure of the envelope from the relatively complete, spherically symmetric distribution seen around AGB stars, to one in which the envelope has been hollowed out by dissociating and ionizing radiation and/or shaped by the action of jet outflows (see Section 1) into bi-cones, rings, tori, etc., which may be oriented at different angles to the line of sight. Red-blue asymmetries in the profiles then arise from back-front asymmetries in the distribution of molecular gas. A second effect is the likely decrease in the opacity of the CO line as the CO is destroyed. A third effect is the size of the PN cavity relative to the telescope beam size. If the third effect were dominant, one would expect that the profile shapes would be correlated with the angular diameter of the PNe. 068.3–02.1 is among the smallest PNe ($1.3''$ Aaquist & Kwok 1990), and is the case with the most parabolic profile, consistent with the emission arising in a relatively undisturbed envelope. However, there is no general correlation between the profile shapes and the angular sizes of the ionized nebulae for the sample as a whole. The prevalence of asymmetries, and strongly double-peaked profiles even among small nebulae, suggest that the structural effects in the envelopes are of major importance.

A second, striking feature of the CO spectra is the large widths of the lines. The distribution of ΔV listed in Table 1 is shown in Fig. 2, where the lower limits for ΔV obtained from Gaussian fits are included. For comparison, Fig. 2 also shows the distribution of CO line widths (twice the expansion velocity) of the sample of 65 bright C-rich AGB stars reported by Olofsson et al. (1993); the distribution of the widths of OH/IR stars is similar as discussed in that paper. The difference between PNe and AGB line widths is clear from

the figure. High velocity gas is rarely seen in AGB envelopes (median width = 25 km s^{-1}), but is the norm in PNe envelopes (median width $\gtrsim 45 \text{ km s}^{-1}$).

The expansion velocity of the ionized gas in PNe is also larger than the expansion velocity of AGB envelopes, typically by a factor of about two. The mean expansion velocities given for PNe in the catalog of Weinberger (1989) are 20.3 km s^{-1} for [O III] and 22.5 km s^{-1} for [N II], and the corresponding line widths fall near the center of the distribution of CO line widths shown in Fig. 2. In PNe the large expansion velocities of the ionized gas are usually ascribed to acceleration by the pressure in the nebulae caused by photo-ionization or fast winds. In the case of the CO lines, the large line widths of the PN spectra in Fig. 1 are mostly formed by extended line wings, e.g., M 1-59 (023.9–02.3). Similar wings are commonly seen in proto-PNe before the onset of ionization, and in the few cases of young PNe where the CO line wings have been studied at high angular resolution, e.g., M 1-16 (Huggins et al. 2000) and He 3-1475 (Huggins et al. 2004), it is found that the wings arise from molecular gas entrained in the sides of high velocity jets. Thus although the kinematics of the molecular gas may be affected by thermal pressure in the ionized gas, the frequency with which wings are seen in the CO spectra reported here probably reflects the frequency of jets in PN formation.

In a few of the cases reported here, the whole CO line appears to be broadened. The most extreme case is K 3-17 (039.8+02.1) which shows a steep-sided, roughly flat-topped profile (with some IS contamination near the center) that is 90 km s^{-1} wide. This profile is unique among PNe and the object deserves further study.

6. Conclusions

This paper reports a sensitive survey of CO emission in PNe. 110 PNe were observed and 40 were detected. The success of the survey demonstrates the usefulness of array receivers for observing CO in PNe or other small sources lying close to the Galactic plane. The results substantially extend the available data on the molecular gas in PNe for statistical study, and provide individual cases for further detailed observation.

We thank the staff of the IRAM 30 m telescope for help with the observations. This work has been supported in part by NSF grants AST 99-86159 and AST 03-07277 (PJH), and by the Spanish MEC under grants AYA2003-7584 (RB), ESP2003-04957 and FEDER grants (PP).

REFERENCES

- Aaquist, O. B., & Kwok, S. 1990, *A&AS*, 84, 229
- Acker, A., Ochsenbein, F., Stenholm, B., Tyllenda, R., Marcout, J., & Schohn, C. 1992, *The Strasbourg-ESO Catalog of Galactic Planetary Nebulae* (Garching: ESO)
- Bachiller, R., Huggins, P. J., Cox, P., & Forveille, T. 1994, *A&A*, 281, 93
- Bachiller, R., Forveille, T., Huggins, P. J., & Cox, P. 1997, *A&A*, 324, 1123
- Bujarrabal, V., Castro-Carrizo, A., Alcolea, J., & Sánchez Contreras, C. 2001, *A&A*, 377, 868
- Condon, J. J., & Kaplan, D. L. 1998, *ApJS*, 117, 361
- Corradi, R. L. M., Gonçalves, D. R., Villaver, E., Mampaso, A., Perinotto, M. Schwarz, H. E., & Zanin, C. 2000, *ApJ*, 535, 823
- Cox, P., Huggins, P. J., Maillard, J. -P., Muthu, C., Bachiller, R., & Forveille, T. 2003, *ApJ*, 586, L87
- Dayal, A., & Bieging, J. H. 1996, *ApJ*, 472, 703
- Dinerstein, H. L., Sneden, C., & Uglum, J. 1995, *ApJ*, 447, 262
- Durand, S., Acker, A., & Zijlstra, A. 1998, *A&AS*, 132, 13
- Gesicki, K., & Zijlstra, A. A. 2000, *A&A*, 358, 1058
- Gomez, Y., Rodriguez, L. F., & Garay, G. 1992, *A&A*, 258, 469
- Guerrero, M. A., Vazquez, R., & Lopez, J. A. 1999, *AJ*, 117, 967
- Gussie, G. T., & Taylor, A. R. 1995, *MNRAS*, 273, 801
- Huggins, P. J., & Healy, A. P. 1989, *ApJ*, 346, 201
- Huggins P. J., Bachiller R., Cox P., & Forveille T. 1996, *A&A*, 315, 284
- Huggins, P. J., Forveille, T., Bachiller, R., & Cox, P. 2000, *ApJ*, 544, 889
- Huggins, P. J., Muthu, C., Bachiller, R., Forveille, & Cox, P. 2004, *A&A*, 414, 581
- Huggins, P. J., & Manley, S. P. 2005, *PASP*, in press
- Josselin, E., & Bachiller, R., 2001, *A&A*, 376, 484
- Kaler, J. B., & Jacoby, G. H. 1991, *ApJ*, 372, 215
- Kastner, J. H., Weintraub, D. A., Gatley, I., Merrill, K. M., & Probst, R. G. 1996, *ApJ*, 462, 777
- Li, J., Harrington, J. P., & Borkowski, K. J. 2002, *AJ*, 123, 2676

- Liu, X., -W. et al. 2001, MNRAS, 323, 343
- Lopez, J. A. 2003, in Planetary Nebulae: Their Evolution and Role in the Universe, IAU Symposium 209, ed. S. Kwok, M. Dopita, & R. Sutherland (San Francisco: ASP), 483
- Lopez-Martin, L., et al. 2002, A&A, 388, 652
- Miranda, L. F., et al. 2000, MNRAS, 311, 748
- Miranda, L. F., Gomez, Y., Anglada, G., & Torrelles, J. M. 2001, Nature, 414, 284
- O’Dell, C. R., Balick, B., Hajian, A. R., Henney, W. J., & Burkert, A. 2002, AJ, 123, 3329
- Olofsson, H., Eriksson, K., Gustafsson, B., & Carlstrom, U. 1993, ApJS, 87, 267
- Phillips, J. P. 2002, ApJS, 139, 199
- Rodriguez, L. F., Goss, W. M., & Williams, R. 2002, ApJ, 574, 179
- Sahai, R., & Trauger, J. T. 1998, AJ, 116, 1357
- Webster, B. L. 1975, MNRAS, 173, 437
- Weinberger, R. 1989, A&AS, 78, 301
- Young, K., Cox, P., Huggins, P. J., Forveille, T., & Bachiller, R. 1999, ApJ, 522, 387
- Zhang, H.-Y., Sun, J., & Ping, J.-S. 2000, Ch. A&A, 24, 309
- Zijlstra, A. A., Pottasch, S. R., & Bignell, C. 1989, A&AS, 79, 329
- Zijlstra, A. A., Chapman, J. M., te Lintel Hekkert, P., Likkell, L., Comeron, F., Norris, R. P., Molster, F. J., & Cohen, R. J. P. 2001, MNRAS, 322, 280

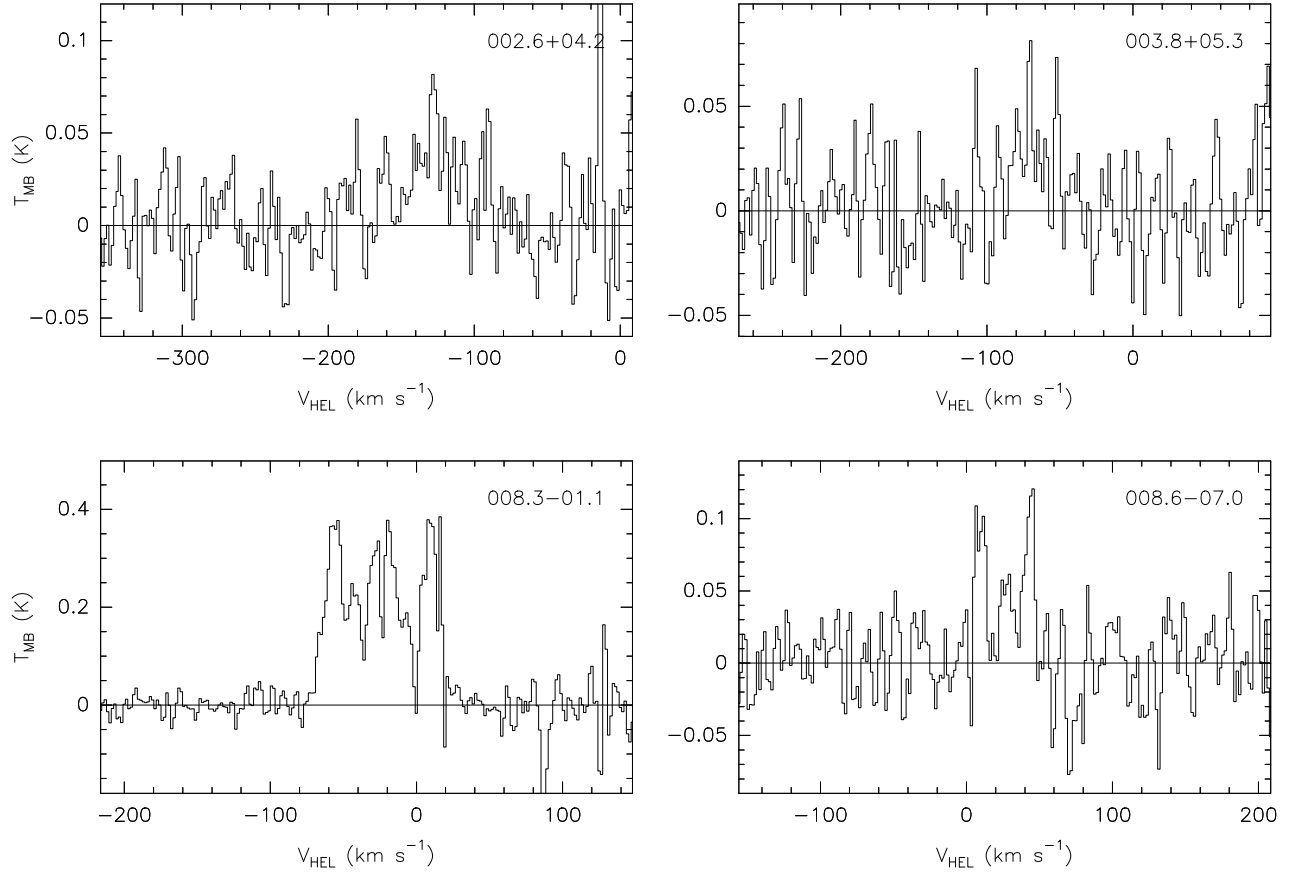


Fig. 1.— CO $J = 2 - 1$ spectra of the PNe detected in the survey. The PNe are identified by the galactic name in each panel and are ordered by Galactic longitude. See section 4 for comments on individual spectra.

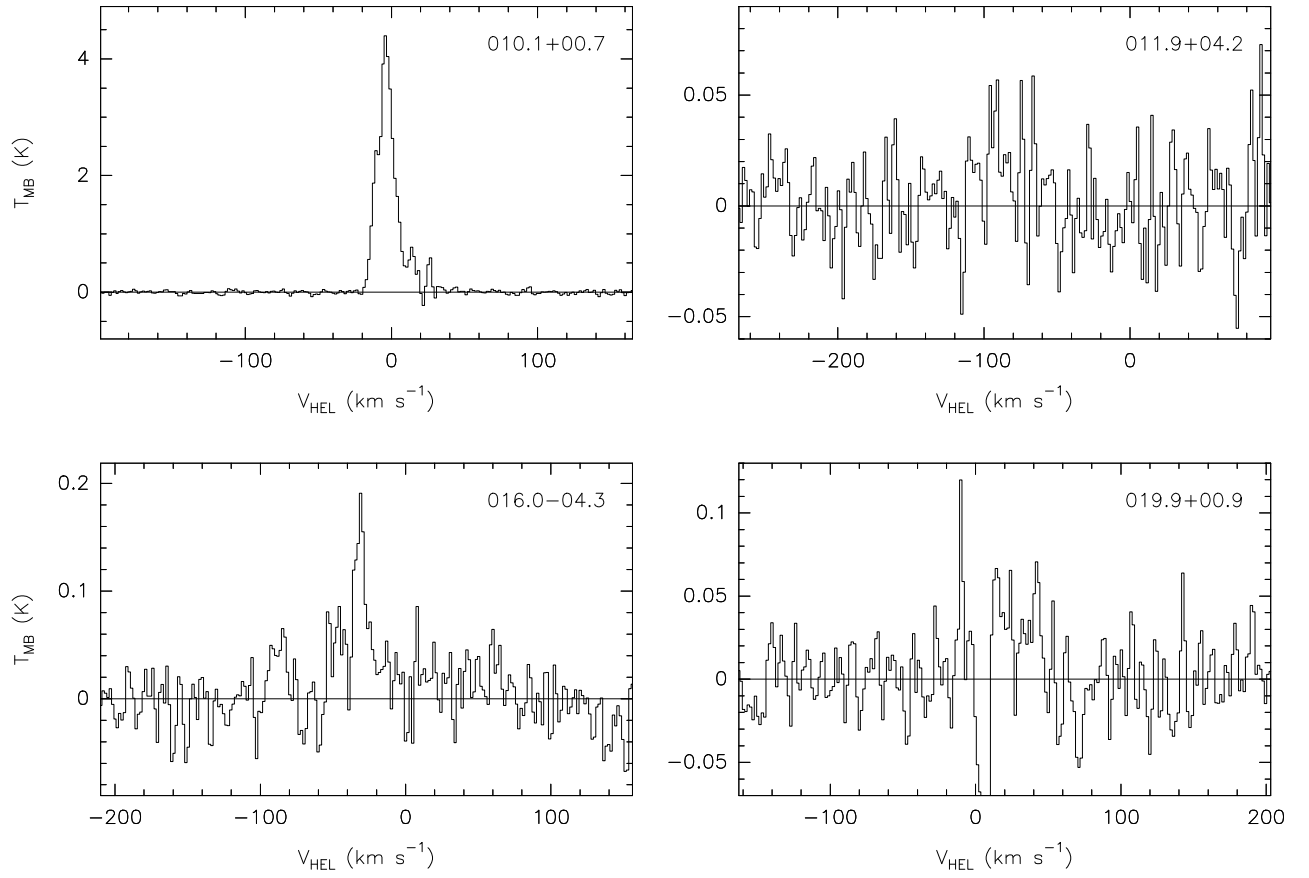


Fig. 1.— continued

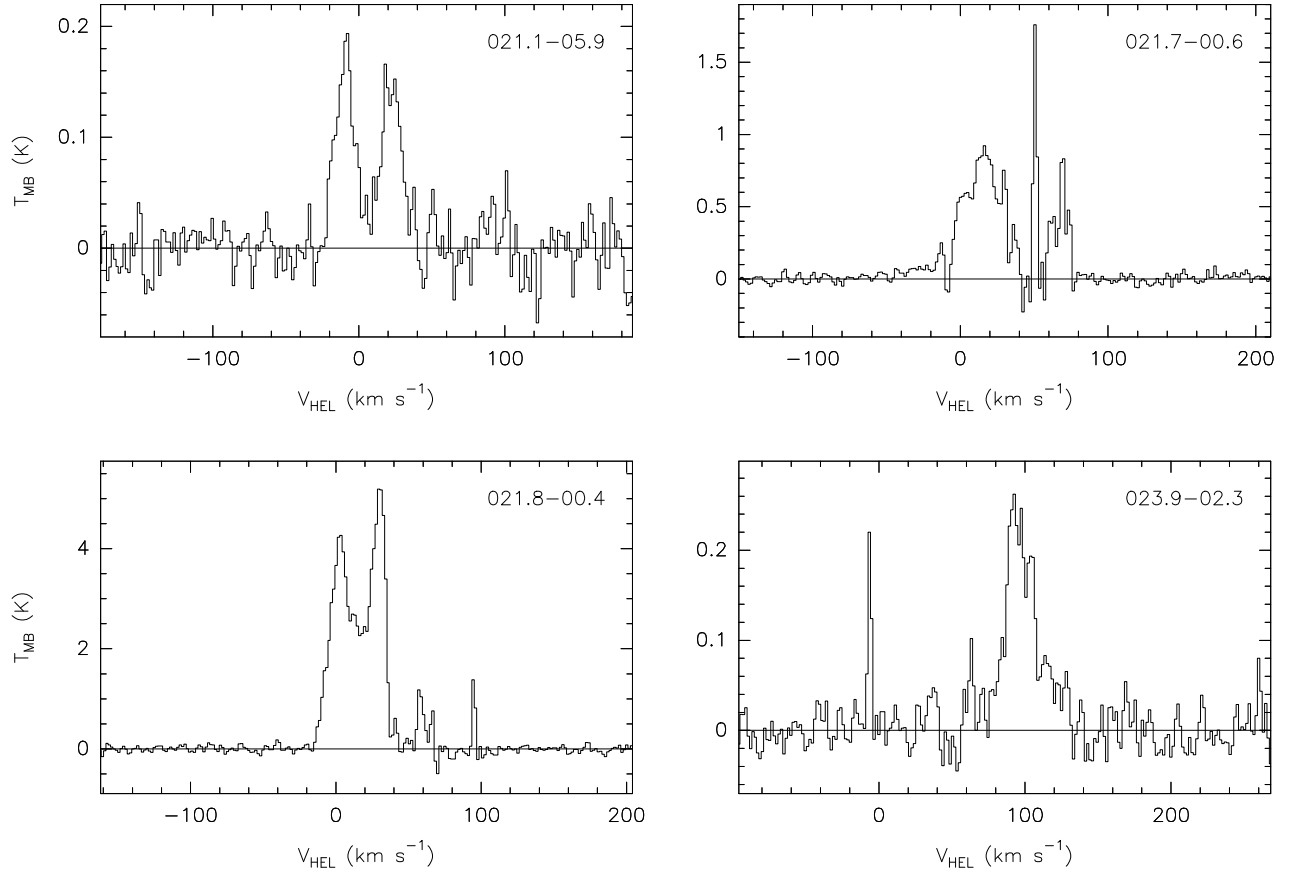


Fig. 1.— continued

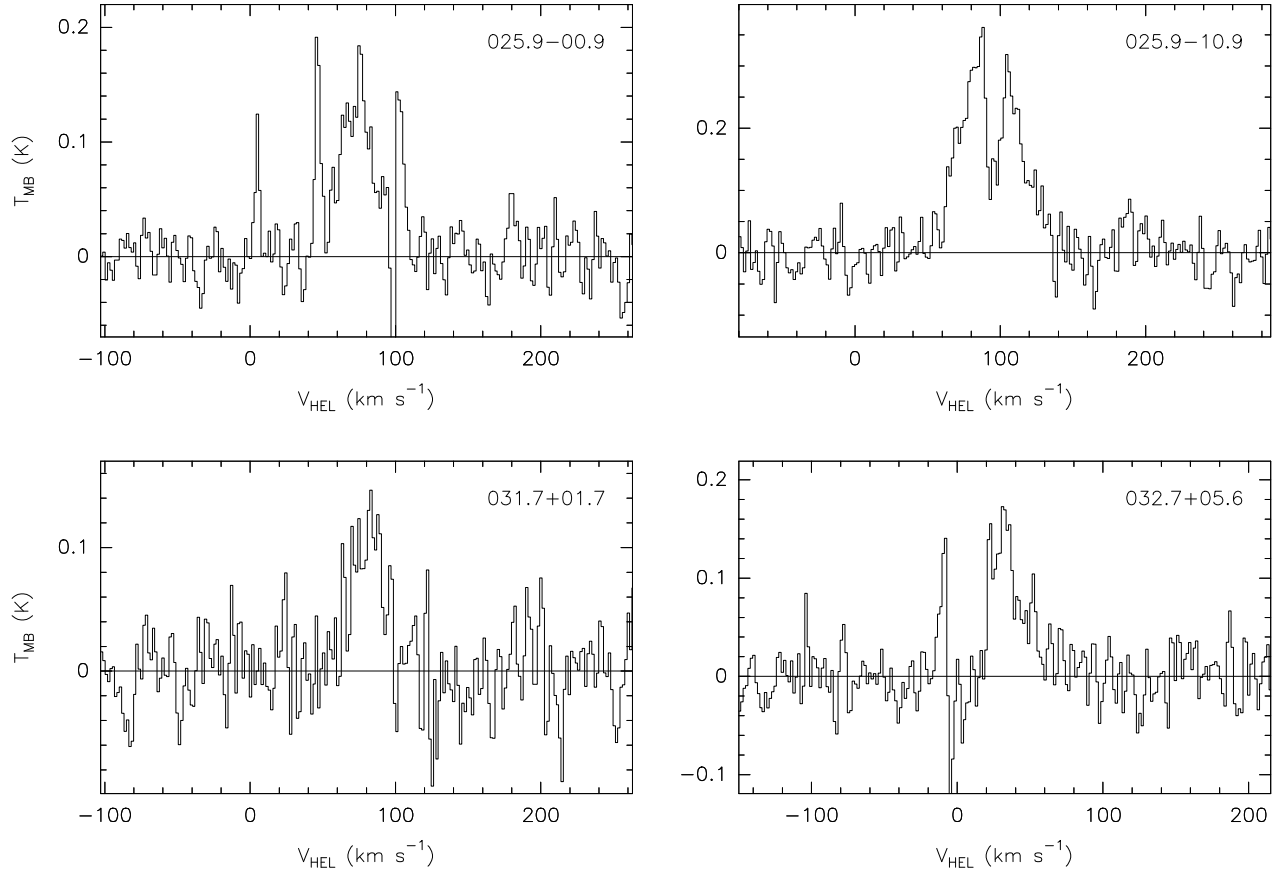


Fig. 1.— continued

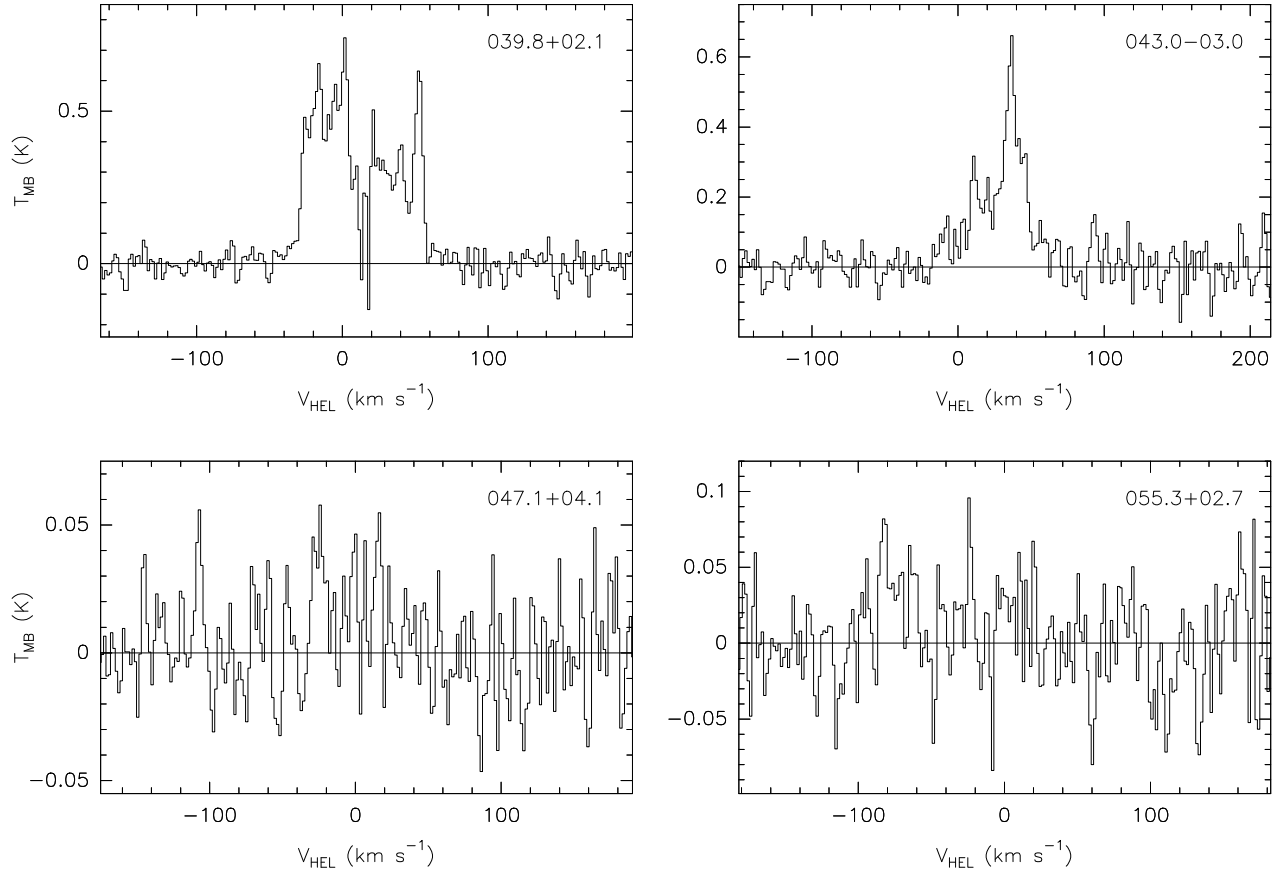


Fig. 1.— continued

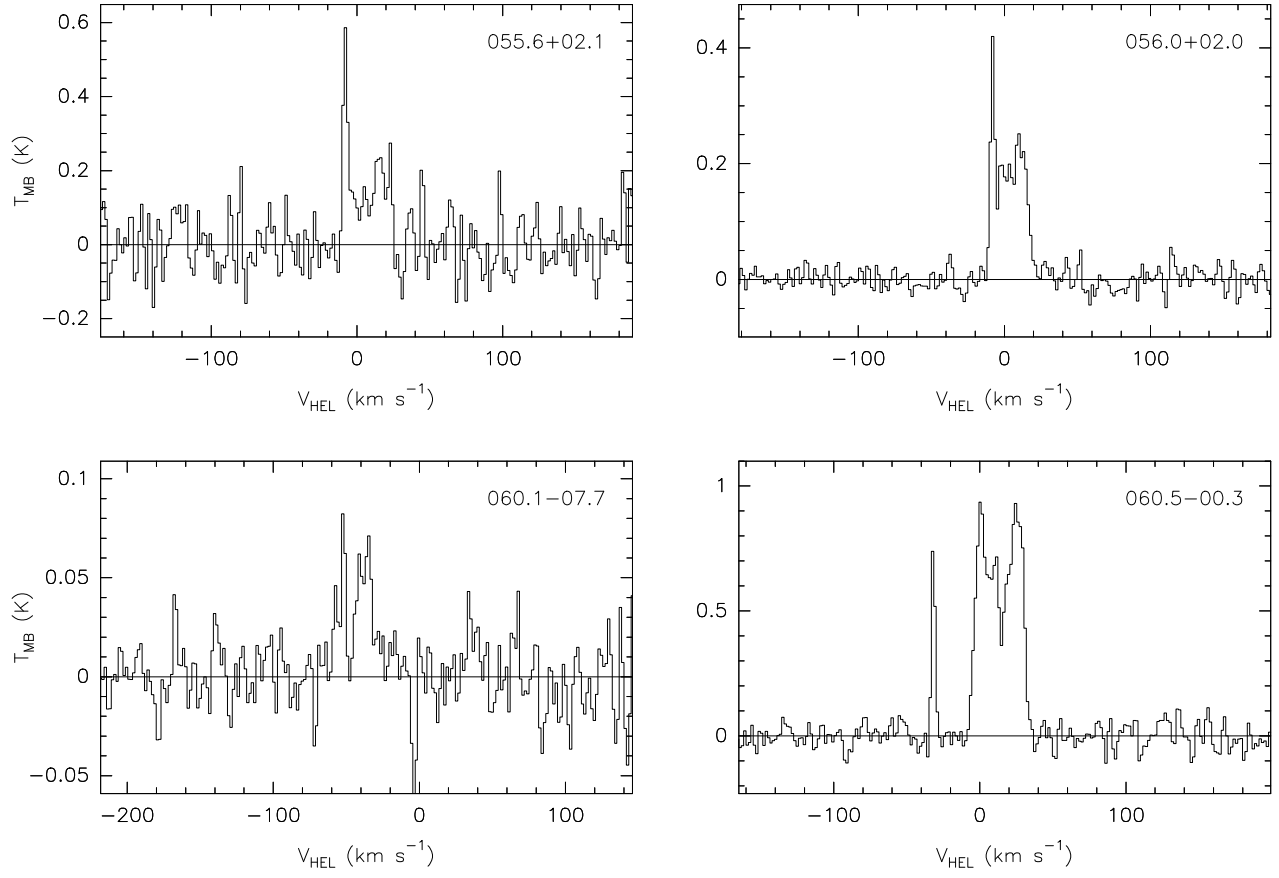


Fig. 1.— continued

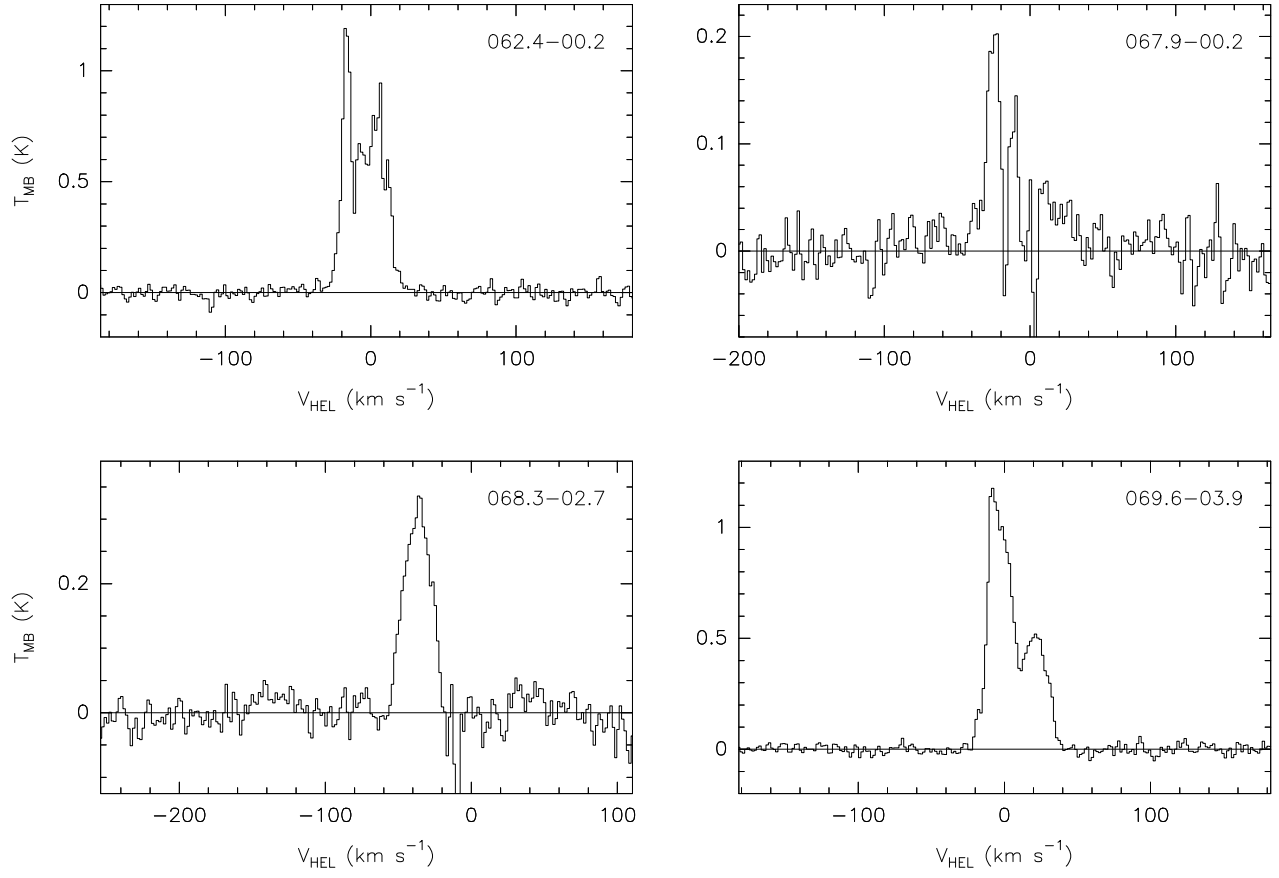


Fig. 1.— continued

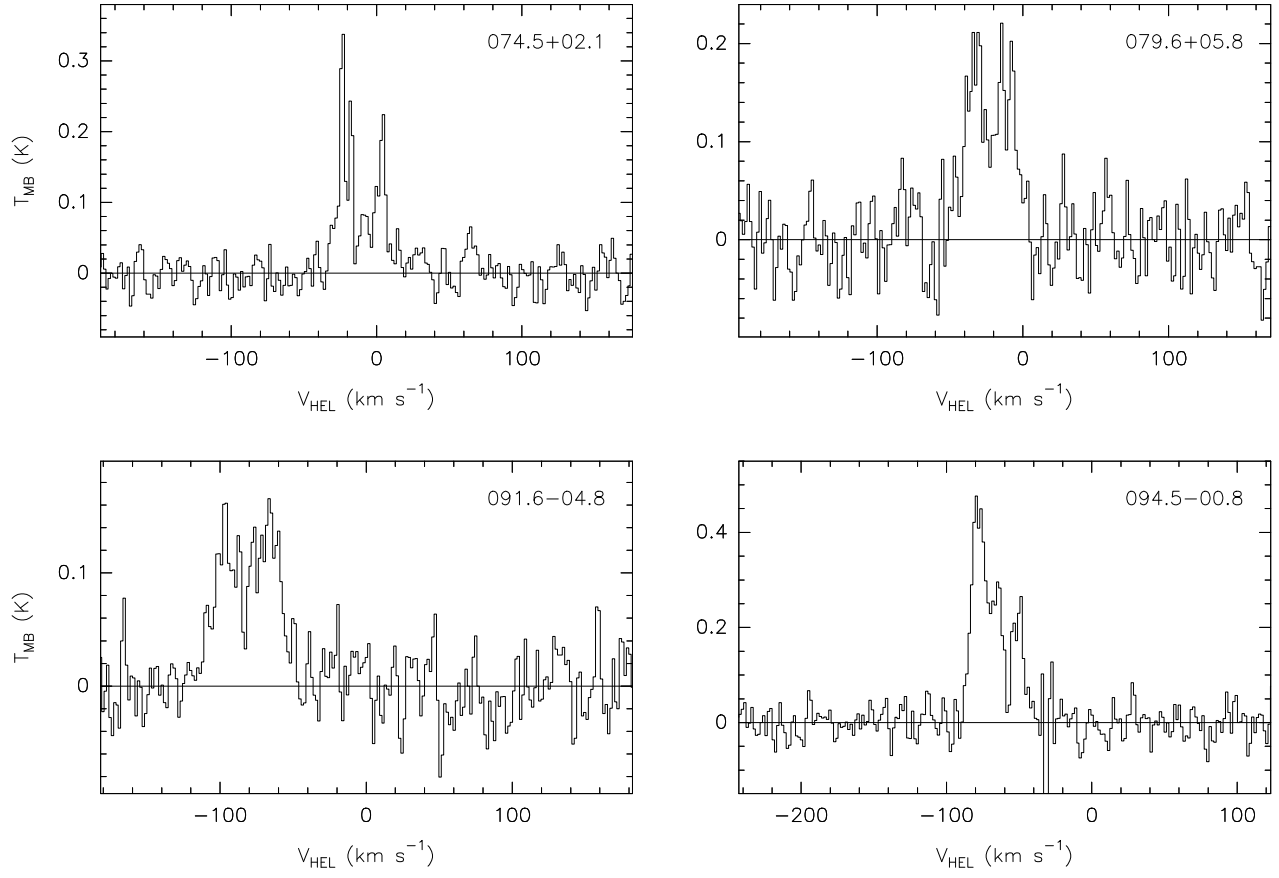


Fig. 1.— continued

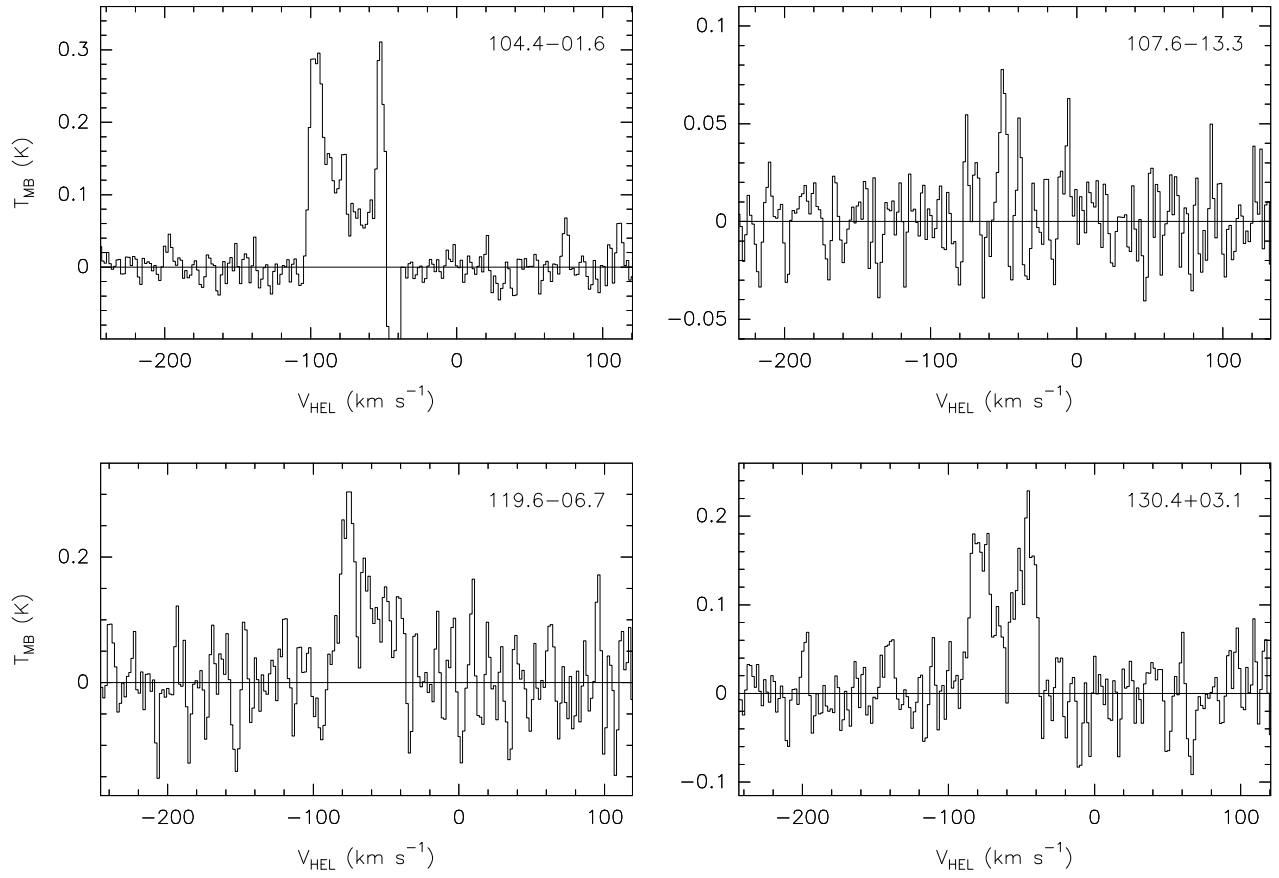


Fig. 1.— continued

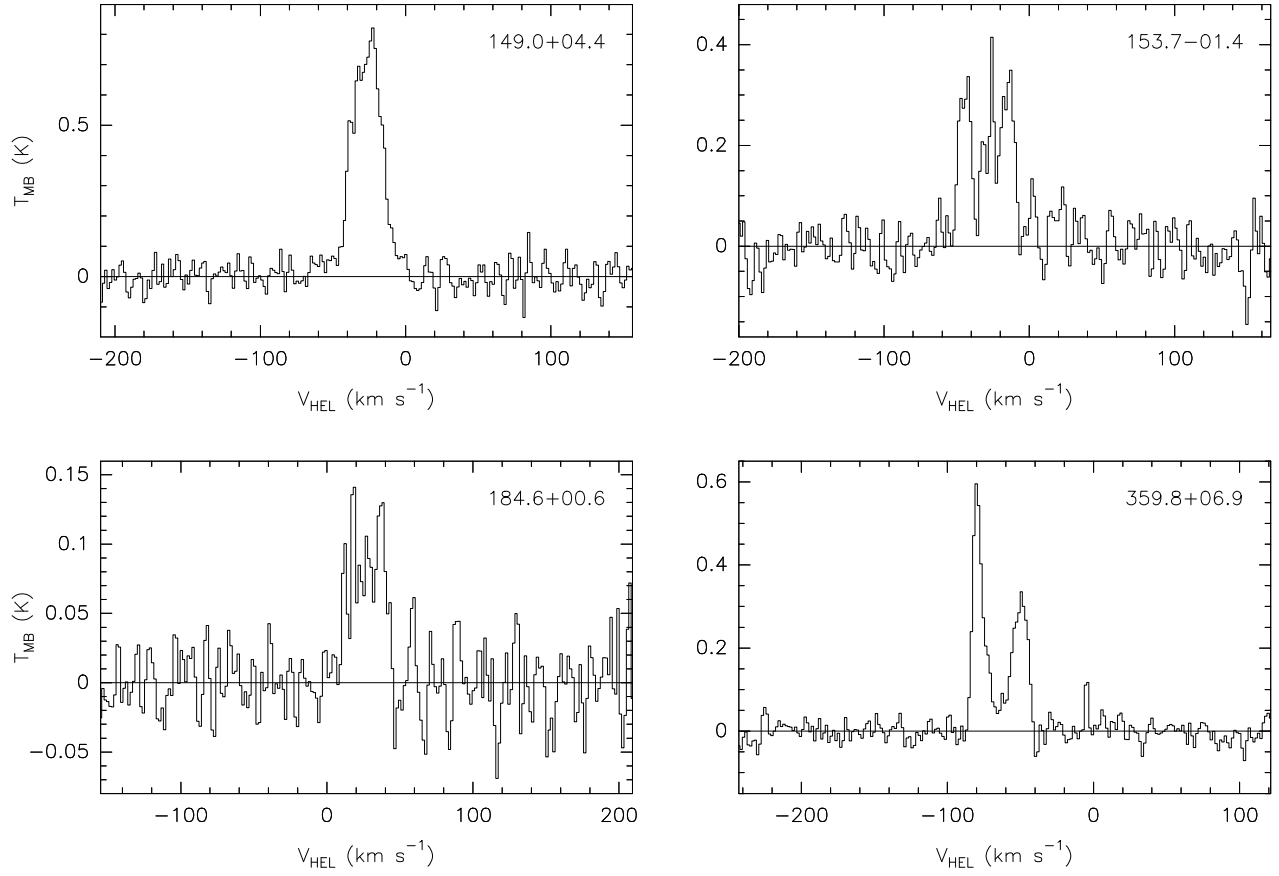


Fig. 1.— continued

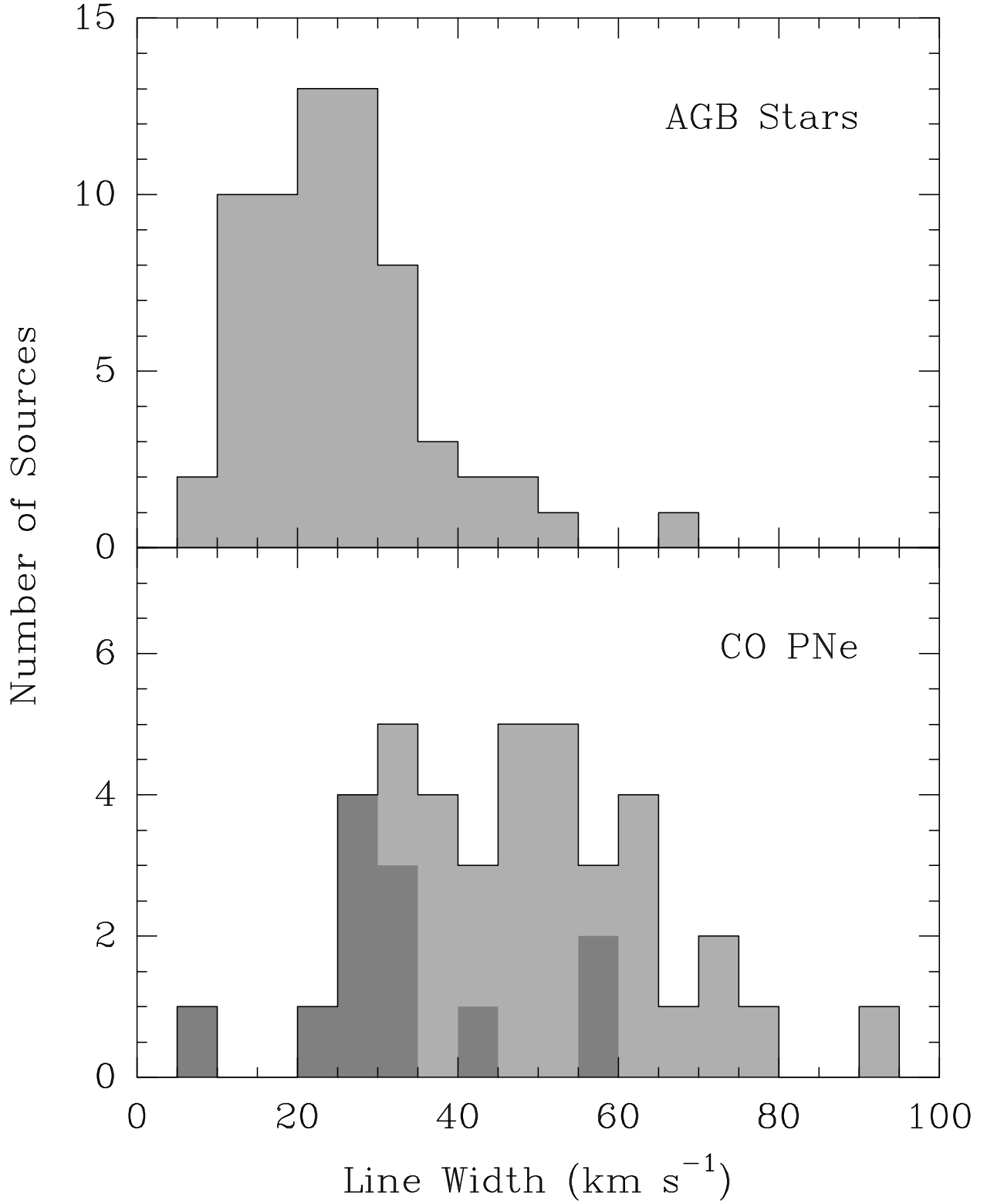


Fig. 2.— Line width comparison of PNe and AGB stars. *Lower panel*: Distribution of the CO line widths of the PNe detected in the survey. The darker regions denote lower limits to the CO widths. *Upper panel*: Distribution of the CO line widths of 65 bright carbon stars. Data from Olofsson et al. (1993).

Table 1. CO Survey of Young Planetary Nebulae

PN	Name	rms (mK)	I (K km s ⁻¹)	V_o (km s ⁻¹)	ΔV (km s ⁻¹)	T_p (mK)	V_{IS} (km s ⁻¹)	Comments
000.1+17.2	PC 12	25	n, g1
000.7+04.7	H 2-11	47	-12 +11	n, g1
002.6+02.1	Te 1580	43	-18 -4	n, g3
002.6+04.2	Th 3-27	21	2.4	-127	>55	40	-17 +9	t, g2
002.8+01.7	H 2-20	27	-20 -3	n, g1
002.8+01.8	Te 1567	30	-15 -4, +15 +19	n, g2
003.6+03.1	M 2-14	29	-6 -3	n, g1
003.8+05.3	H 2-15	24	1.2	-69	>32	36	...	t, g2
004.9+04.9	M 1-25	45	+44 +48, +94 +100	n, g1
006.0+03.1	M 1-28	33	-22 -12	n, g4
006.3+03.3	H 2-22	32	-57 -36, -16 -5	n, g1
006.4+02.0	M 1-31	41	-5 +1	n, g3
006.5-03.1	H 1-61	35	-3 +2	n, g1
006.7-02.2	M 1-41	24	-100 +25	n, g2, s
007.2+01.8	Hb 6	30	+3 +12	n, g3
007.8-04.4	H 1-65	27	n, g1
008.3-01.1	M 1-40	22	15.8	-35	70	360	-25 +20, +84 +145	d, g2, s
008.3-07.3	NGC 6644	27	n, g3
008.6-07.0	He 2-406	26	2.4	+27	50	100	...	d, g2
010.1+00.7	NGC 6537	31	59.7	-4	30	4340	+1 +34, +88 +95	d, g2
010.7-06.4	IC 4732	24	n, g3
011.0+05.8	NGC 6439	46	n, g3
011.1+11.5	M 2-13	49	n, g3
011.9+04.2	M 1-32	19	0.77	-90	>27	27	-10 -6	t, g1
012.6-02.7	M 1-45	31	+41 +63	n, g1
013.4-03.9	M 1-48	41	n, g2
014.9-03.1	SaSt 3-16	29	n, g1
015.9+03.3	M 1-39	23	+0 +9	n, g1
016.0-04.3	M 1-54	26	2.8	-32	>23	110	...	d, g2
016.4-01.9	M 1-46	42	+23 +45	n, g1
018.9+04.1	M 3-52	32	-6 -1	n, g2
019.7-04.5	M 1-60	28	-14 +0	n, g3
019.9+00.9	M 3-53	19	1.8	+18	>41	40	-10 +10, +22 +26	d, g2
020.9-01.1	M 1-51	43	-14 +80	n, g4, s
021.1-05.9	M 1-63	22	5.6	+6	60	170	...	d, g2
021.7-00.6	M 3-55	31	30.0	+16	46	838	-17 -4, +23 +71	d, g1, s

Table 1—Continued

PN	Name	rms (mK)	I (K km s ⁻¹)	V_o (km s ⁻¹)	ΔV (km s ⁻¹)	T_p (mK)	V_{IS} (km s ⁻¹)	Comments
021.8–00.4	M 3-28	62	147.1	+17	52	5160	–11 +99	d, g2
022.1–02.4	M 1-57	33	–9 –3, +17 +21	n, g2
023.3–07.6	MaC 1-16	43	n, g2
023.9–02.3	M 1-59	21	6.0	+97	63	220	–8 –2	d, g3
024.1+03.8	M 2-40	22	–13 –2	n, g1
024.3–03.3	Pe 1-17	28	–8 –1, +38 +45	n, g2
024.8–02.7	M 2-46	29	–11 –2, +40 +49	n, g1
025.9–00.9	Pe 1-14	20	4.2	+74	>32	124	+5 +49, +74 +105	d, g2, s
025.9–10.9	Na 2	33	13.5	+95	73	290	...	d, g2
028.5+05.1	K 3-2	29	–17 –14	n, g1
031.7+01.7	PC 20	31	3.2	+81	>26	116	–15 –1	d, g3
032.5–03.2	K 3-20	40	–10 –5	n, g1
032.7+05.6	K 3- 4	26	3.5	+33	36	144	–18 +0	d, g3
034.0+02.2	K 3-13	42	–5 +1	n, g3
036.9–01.1	HaTr 11	41	–6 +3	n, g4
038.2+12.0	Cn 3-1	29	n, g1
038.4–03.3	K 4-19	40	–11 –5	n, g1
039.8+02.1	K 3-17	39	34.2	+15	90	610	–1 +22	d, g3
042.0+05.4	K 3-14	36	n, g4
043.0–03.0	M4-14	52	14.5	+24	76	610	–77 –7	d, g2
043.1+03.8	M 1-65	60	–1 +16	n, g1
045.9–01.9	K 3-33	35	–14 –7, +7 +14	n, g1
047.1+04.1	K 3-21	17	1.3	–4	>58	21	...	t, g2
048.1+01.1	K 3-29	73	+13 +21	n, g3
048.7+01.9	He 2-429	21	–73 –60, –14 –1	n, g3
049.4+02.4	He 2-428	38	–14 –3	n, g1
051.0+03.0	He 2-430	40	–6 +3	n, g3
051.9–03.8	M 1-73	24	–1 +2	n, g1
052.5–02.9	Me 1-1	25	n, g3
055.3+02.7	He 1-1	32	1.3	–77	>26	47	–73 –70, –11 –8	t, g2
055.5–00.5	M 1-71	51	+17 +27	n, g3
055.6+02.1	He 1-2	74	5.0	+7	35	200	–12 –6	d, g1
056.0+02.0	K 3-35	18	5.7	+3	31	220	–13 –6	d, g2
057.9–01.5	He 2-447	28	–3 +2, +17 +20	n, g1
058.3–10.9	IC 4997	19	n, g1
059.0+04.6	K 3-34	32	n, g2

Table 1—Continued

PN	Name	rms (mK)	I (K km s ⁻¹)	V_o (km s ⁻¹)	ΔV (km s ⁻¹)	T_p (mK)	V_{IS} (km s ⁻¹)	Comments
059.9+02.0	K 3-39	92	-13 -8	n, g1
060.1-07.7	NGC 6886	16	1.4	-42	>28	46	-6 -2	d, g3
060.5-00.3	K 3-45	46	25.6	+15	43	870	-35 -28, +14 +27	d, g1
060.5+01.8	He 2-440	33	n, g1
061.3+03.6	He 2-437	24	n, g1
062.4-00.2	M 2-48	26	25.1	-4	51	1170	-13 +13	d, g2
066.9+02.2	K 4-37	26	-1 +5	n, g4
067.9-00.2	K 3-52	19	4.7	-25	67	190	-29 +6	d, g1
068.3-02.7	He 2-459	24	7.2	-37	35	330	-17 -2	d, g1
068.8-00.0	M 1-75	26	-29 +2	n, g4, s
069.2+02.8	K 3-49	37	n, g1
069.2+03.8	K 3-46	30	n, g4
069.6-03.9	K 3-58	19	31.4	+8	61	1150	-12 -7	d, g2
074.5+02.1	NGC 6881	23	4.9	-12	43	150	-30 -15	d, g3
077.7+03.1	KjPn 2	51	-22 -17	n, g2
078.9+00.7	Sd 1	69	-40 +0	n, g1, s
079.6+05.8	M 4-17	34	6.2	-23	51	170	-10 -6	d, g4
082.1+07.0	NGC 6884	20	n, g3
084.2+01.0	K 4-55	30	-89 -53, -26 -11	n, g4
091.6-04.8	K 3-84	28	6.5	-80	63	130	...	d, g2
092.1+05.8	K 3-79	29	-23 -15	n, g3
094.5-00.8	K 3-83	33	10.8	-66	45	420	-63 -44, -33 -27	d, g2
103.7+00.4	M 2-52	23	-84 -49	n, g4
104.4-01.6	M 2-53	20	7.8	-74	55	290	-38 -48	d, g4
107.6-13.3	Vy 2-3	17	0.40	-51	>5	80	...	t, g3
107.7-02.2	M 1-80	32	n, g3
111.2+07.0	KjPn 6	23	-70 -66, -11 -7	n, g1
119.6-06.7	Hu 1-1	60	6.8	-68	>33	190	...	d, g3
129.5+04.5	K 3-91	49	n, g1
130.3-11.7	M 1-1	25	n, g1
130.4+03.1	K 3-92	33	6.5	-62	50	180	-13 -10	d, g3
149.0+04.4	K 4-47	44	19.7	-27	49	780	...	d, g2
153.7-01.4	K 3-65	44	9.3	-30	45	290	-29 -23	d, g3
165.5-06.5	K 3-67	33	+0 +4	n, g3
167.4-09.1	K 3-66	27	+8 +15	n, g1
184.6+00.6	K 3-70	24	2.7	+27	35	96	...	d, g2

Table 1—Continued

PN	Name	rms (mK)	I (K km s ⁻¹)	V_o (km s ⁻¹)	ΔV (km s ⁻¹)	T_p (mK)	V_{IS} (km s ⁻¹)	Comments
204.8–03.5	K 3-72	48	n, g1
359.8+06.9	M 3-37	25	9.9	–65	45	560	–9 –1	d, g2

Note. — Column [9]: d, detection; n, non-detection; t, tentative detection; g1–4, spectroscopic group; s, severe interstellar contamination